

# Supersonic Cloud Collision - II

S. V. Anathpindika<sup>1\*</sup>

<sup>1</sup> *School Of Astronomy and Physics, Cardiff University, 5-The Parade, CF24 3AA*

Accepted 0000 December 00. Received 0000 December 00; in original form 0000 October 00

## ABSTRACT

In this, second paper of the sequel of two papers, we present five SPH simulations of fast head-on cloud collisions and study the evolution of the ram pressure confined gas slab. Anathpindika (2008) (hereafter paper I) considered highly supersonic cloud collisions and examined the effect of bending and shearing instabilities on the shocked gas slab. The post-collision shock here, as in paper I, is also modelled by a simple barotropic equation of state (EOS). However, a much stiffer EOS is used to model the shock resulting from a low velocity cloud collision. We explore the parameter space by varying the pre-collision velocity and the impact parameter.

We observe that pressure confined gas slabs become Jeans unstable if the sound crossing time,  $t_{cr}$ , is much larger than the freefall time,  $t_{ff}$ , of putative clumps condensing out of them. Self gravitating clumps may spawn multiple/larger  $N$ -body star clusters. We also suggest that warmer gas slabs are unlikely to fragment and may end up as diffuse gas clouds.

**Key words:** Molecular clouds (MCs) – pressure compressed gas slab – gravitational instabilities – filaments – star formation – SPH.

## 1 INTRODUCTION

*Star clusters and their birth* : Certain features of star formation are now clear. It has been observationally well established that most star formation occurs in clusters (e.g. Pudritz 2002). There are two paradigms of star formation, one that of collapsing MCs - the cloud - core picture (Hoyle 1953; Whitworth *et al* 1996) and second, the dynamical picture of star formation also called, triggered star formation.

The former picture is elucidated by the growth of gravitational perturbations in the galactic disk or compression of MCs by spiral or bar density waves. Such theories are encouraged by spatial correlation between star formation and the spiral arms of disk galaxies. Gravitational perturbations grow in regions which become Toomre unstable. Further, the surface density in star forming regions,  $\Sigma_{gas}$ , is supposedly related to the star formation rate (SFR),  $\Sigma_{SFR}$ , through a power-law

$$\Sigma_{SFR} \propto \Sigma_{gas}^N, \quad (1)$$

where  $N = 1.4 \pm 0.15$  (Schmidt 1959; Kennicutt 1989; Kennicutt, 1998). Note that  $\Sigma_{gas}$  and  $\Sigma_{SFR}$ , are averaged over the galactic disk.

Kennicutt (1998) also showed that  $\Sigma_{SFR}$  is correlated with the orbital frequency,  $\Omega$ , as

$$\Sigma_{SFR} \propto \Sigma_{gas}\Omega. \quad (2)$$

Note that these correlations, equations (1) and (2), are valid over five orders of magnitude. Yet others, for e.g. Wyse (1986) and Wyse & Silk (1989) have suggested a similar correlation

$$\Sigma_{SFR} \propto \Sigma_{gas}^N(\Omega - \Omega_p), \quad (3)$$

where  $\Omega_p$  is the pattern frequency of the spiral density wave. We recover equation 1, in the limit of small  $\Omega_p$  and  $N = 1$ .

This paradigm, inevitably, leads to a correlation between the SFR and density wave amplitude however, there is no corroborative observational evidence (e.g. Elmegreen & Elmegreen 1986; Kennicutt 1989). Another difficulty with this paradigm is the failure to reconcile the evidence for star formation in those spirals, which have small density wave amplitude (e.g. Block *et al* 1994). Such galaxies, like other spiral galaxies, also show evidence for existence of MCs and star formation. This suggests that the spiral density waves and disk instabilities are not quintessential to star formation. We may therefore have to explore certain aspects of the second paradigm, stated above. Tan (2000) for instance, invoked cloud collision in the SFR calculations for a galactic disk and arrived at a power-law correlation similar to the one given by equation (1).

Triggered star formation is a self regulatory process. Rich, young star clusters have been observationally well studied. The orbital dynamics of clusters have enabled observers to estimate various physical properties of multiple

\* E-mail: Sumedh.Anathpindika@astro.cf.ac.uk(SVA)

**Table 1.** List of simulations performed with relevant physical details.

Serial No.	Experimental details	Precollision Mach Number( $\mathcal{M}$ )	Number of particles	Head-on	$T_{ps}$
1	$M_{cld1} = M_{cld2} = 50 M_{\odot}$ $R_{cld1} = R_{cld2} = 0.8$ pc, T = 54 K	3	$N_{gas} = 120000$	Yes	54 K
2	$M_{cld1} = M_{cld2} = 50 M_{\odot}$ $R_{cld1} = R_{cld2} = 0.8$ pc, T = 54 K	3	$N_{gas} = 120000$	No	54 K
3	$M_{cld1} = M_{cld2} = 50 M_{\odot}$ $R_{cld1} = R_{cld2} = 0.8$ pc, T = 54 K	3	$N_{gas} = 120000$	Yes	10 K
4	$M_{cld1} = M_{cld2} = 2000 M_{\odot}$ $R_{cld1} = R_{cld2} = 4.5$ pc, T = 377 K	3	$N_{gas} = 120000$	No	10 K
5	$M_{cld1} = M_{cld2} = 50 M_{\odot}$ $R_{cld1} = R_{cld2} = 1$ pc, T = 54 K	1	$N_{gas} = 120000$	Yes	54 K

Note : The numbers on the left hand side below indicate the respective column numbers of the table.

(2) Physical details of individual clouds in a simulation (Mass, radius and temperature of individual clouds).

(3) Precollision Mach number ( $\mathcal{M}$ ).

(4) Number of gas particles ( $N_{gas}$ ) used in the simulations.

(5) Post-shock temperature  $T_{ps}$  set in the EOS (see equations (4) and (5)).

systems like orbital eccentricities and orbital stability, stellar masses, among other properties. Star clusters have reasonably homogeneous environs and therefore, are useful regions to study stellar evolution. For a more detailed review of the matter refer Clarke, Bonnell & Hillenbrand (2000).

Star clusters however, show a wide variation in stellar density. For instance,  $\sim 96$  percent of the IR sources in the Orion B region are distributed over four identified star forming regions. On the other hand, in the Orion A region, star forming cores are distributed along the north-south direction - the Integral shaped filament e.g. Lada *et al* (1991); Meyer & Lada (1999) and Mookerjee *et al* (2000). These *bursts* (i.e. formation of star clusters) of star formation also play an important role in the dynamics of galactic disks. Numerical simulations by Clarke & Gittins (2006) for instance, suggest that a *burst* event creates local perturbations in the galactic disk which produces spiral patterns in it. Interference of many such perturbations may create complex structure, that evolves over the timescale of a rotational period

*Birth of star clusters - Numerical studies* : Several scenarios of triggered star formation have been suggested and numerically studied. The dynamical turbulence model is one such example. This model envisages collision between turbulent fluid flows leading to shocked dense gas slabs, post-collision. In the thin optical limit, the slab rapidly cools. Such slabs are dominated by thermal, shearing and bending instabilities. See for instance Klessen, Burkert & Bate (1998); Klessen & Burkert (2000).

Another model is that of the fragmentation of dense gas shells swept up by expanding ionising fronts from massive star clusters. These shells evolve through a complex interplay between the non-linear bending instability and the gravitational instability. Subsequently the shells fragment. The dynamical evolution of these shells leads to the formation of dense filaments and clumps (typical densities  $\gtrsim 10^{-6}$  cm $^{-3}$ ). The clumps so formed are usually spheroidal and have turbulent interiors. Clumps located in filaments are fed with material channelled along natal filaments and may eventually become self gravitating. Isolated

clumps on the other hand, either remain quasi stable or suffer tidal disruption. The subject of structure formation and triggered star formation due to expanding ionising radiation from star clusters has been investigated by several workers. See for instance Wada, Spaans & Kim (2000); Curry (2002); Dale, Bonnell, Whitworth (2007); Furuya, Kitamura & Shinnaga (2008); Lefloch, Cernicharo & Pardo (2008) and other related references therein.

The other model suggested and investigated further in the present work, is that of gravitational fragmentation of an external pressure confined gas slab. See for e.g. Elmegreen & Elmegreen (1978), Curry (2002), Whitworth *et al* (1994) and Boyd & Whitworth (2005). These slabs result from clouds colliding with relatively small precollision Mach numbers (Chapman *et al* 1992; Bhattal *et al* 1998).

We investigated one extreme of the cloud collision problem in paper I by simulating highly supersonic, both, head-on and off-centre cloud collisions. We found that the dynamical behaviour of a shock compressed gas slab is dominated by internal shear. Shearing instabilities suppress the gravitational instability. Turbulent mixing between slab layers makes the slab susceptible to the non-linear thin shell instability (NTSI) and the Kelvin-Helmholtz (KH) instability. Further, the internal shear leads to dissipation of thermal energy via shocking between fluid layers. Gradually the slab loses thermal support and collapses under self gravity to form a thin, long filament along the collision axis. This is quite similar to the integral filament in the Orion A region.

In this paper we present five simulations, in that, two each are of fast head-on and off-centre cloud collisions respectively. The remaining one is a slow head-on cloud collision and employs a much stiffer equation of state (EOS). We shall attempt to contrast the findings recorded in paper 1 with those, presented here. The plan of the paper is as follows. In §2 below we introduce the numerical scheme employed for our work and the code used. In §3 we describe the initial conditions and list the simulations performed. The re-

sults are discussed in §4 and we conclude in §5. The column density is measured in  $M_{\odot}\text{pc}^{-2}$  and all the column density plots presented here, are plotted on a logarithmic scale since they span about six orders of magnitude. The spatial coordinates are marked in parsecs.

## 2 THE NUMERICAL METHOD & CODE

We use the Smoothed Particle Hydrodynamics (SPH) numerical method for our simulations. This scheme treats the fluid under investigation as an ensemble of particles. The simulations presented here are performed using an extensively tested SPH code, DRAGON (Goodwin, Whitworth & Ward-Thompson 2004). It uses the Barnes-Hut Octal spatial tree (Barnes & Hut 1986) to search nearest neighbours and, evaluate the net force on a SPH particle. The critical cell opening angle used by us,  $\theta_{crit} \sim 0.45$  and each particle has  $50 \pm 5$  neighbours. In order to improve the accuracy of force calculations quadrupole moments of remote cells are also included. The code employs the multiple particle time stepping scheme (Mookerjee *et al* 2000).

An extremely dense agglomeration of particles in the simulation is replaced by a sink particle. The sink is characterised by two physical variables viz. the sink radius,  $R_{sink}$ , and the sink density,  $\rho_{sink}$ , both of which are predefined (Bate, Bonnell & Price 1995). We set  $\rho_{sink} = 10^{-12} \text{ g cm}^{-3}$  in all the simulations presented here. The sink radius is so chosen that the initial mass of a sink particle is comparable to the minimum resolvable mass in the simulation. In the present work, protostellar cores are modelled as sinks.

## 3 INITIAL CONDITIONS & NUMERICAL EXPERIMENTS

We model MCs as unconfined Bonnor-Ebert spheres. Thus, there is no external pressure on the cloud edges. We compromise with the intercloud medium in these simulations to permit larger number of gas particles in the clouds. The procedure for assembling the two clouds is the same as that described in paper I.

In the first four models tested here, we employ a simple barotropic equation of state (EOS) given as

$$P(\rho) = a^2 \left[ 1 + \left( \frac{\rho}{10^{-14} \text{ g cm}^{-3}} \right)^{\gamma-1} \right], \quad (4)$$

where  $a$  is the sound speed and  $a^2 = \frac{k_B T_{ps}}{\bar{m}_H}$ . Here  $k_B$  and  $\bar{m}_H$  are respectively, the Boltzmann constant and the average mass of a hydrogen atom while  $T_{ps}$  is the post-collision ambient temperature. In models 1 and 2, we set  $T_{ps}$  equal to the temperature in the pre-collision cloud. By so setting the post-collision temperature, we are attempting to model a radiative shock in a rather crude manner. We do so since, the cooling time for a strong shock in astrophysical environs is much smaller than the sound crossing time (refer paper I).

Now, if the post-shock radiative cooling in real shocks is very efficient, the shocked slab would cool to much lower temperatures. In models 3 and 4, we therefore assume a

modest post-shock temperature of 10 K. We have thus, assumed radiative shocks and isothermal gas slabs in these simulations. Admittedly, shocks ought to be treated using radiative cooling schemes however, our emphasis here is on the dynamical evolution of the pressure confined slab.

Finally, following the very low precollision velocity ( $\sim 0.4 \text{ km s}^{-1}$ ) of individual clouds in model 5, the post-collision shock is weak. Weak shocks in astrophysical environs are nearly adiabatic, and so we model one here, with a slightly stiffer EOS given by

$$T = T_{ps} \left( \frac{\rho}{\rho_{ps}} \right)^{\gamma-1}, \quad (5)$$

where  $\rho_{ps}$  is the post-shock gas density obtained from the Rankine-Hugoniot jump conditions for an adiabatic shock and  $T_{ps} = 54 \text{ K}$ , same as the pre-collision cloud temperature. For the physical conditions considered in this model,  $\rho_{ps} = 10^{-21} \text{ g cm}^{-3}$  (which is the average density in pre-collision clouds). The adiabatic gas constant,  $\gamma = \frac{5}{3}$  in either EOSs. Models tested here have been listed in Table 1 above along with their relevant physical details.

## 4 DISCUSSION

The question of gravitational instability in cold, semi-infinite planar gas slabs has been extensively studied in the past. However, most of these analyses were restricted to slabs with no external pressure on them. See for instance, Mestel (1965) and Larson (1985).

The stability analysis of cold, external pressure confined isothermal slabs by Elmegreen & Elmegreen (1978) and Elmegreen (1989) suggests that the minimum mass of a fragment condensing out of such a slab, increases with the age of that slab as it continues to accrete matter. The monotonic growth time of the fastest growing unstable mode in such a slab is  $\sim 0.25(G\rho_{layer})^{-\frac{1}{2}}$  (Elmegreen 1989), where  $\rho_{layer}$  is the average density of the post-shock gas slab.

Expressions for the length of the fastest growing mode, the timescale of growth of this mode and the minimum mass of the fragment condensing out of the slab have been derived by (Whitworth *et al* 1994) and Boyd & Whitworth (2005). Below we discuss the models tested in this work and compare the results of models 3 and 4 with the analytic findings of the latter authors.

### Fast cloud collision ( $T_{ps} = 54 \text{ K}$ ; models 1 & 2)

In model 1 MCs of mass  $50 M_{\odot}$  each, collide head-on with each other at a pre-collision velocity of  $\sim 1.3 \text{ km s}^{-1}$  ( $\mathcal{M} = 3$ ). Individual clouds are thermally supported against self gravity. The post-collision thermodynamics in this model is governed by the EOS defined by equation (4) above. The clouds collide and form a planar gas slab confined by ram pressure. The time sequence of colliding clouds and their evolution after collision is shown in Fig.1, which is a column density plot showing the clouds and the post-collision slab.

We treat the gas slab as approximately isothermal and the post-shock temperature,  $T_{ps}$ , is set equal to the pre-collision cloud temperature. This is obviously under the premise that in the physical world, radiative cooling plays its part efficiently in such shocks. We believe that our assumption should not have any adverse bearing on the final

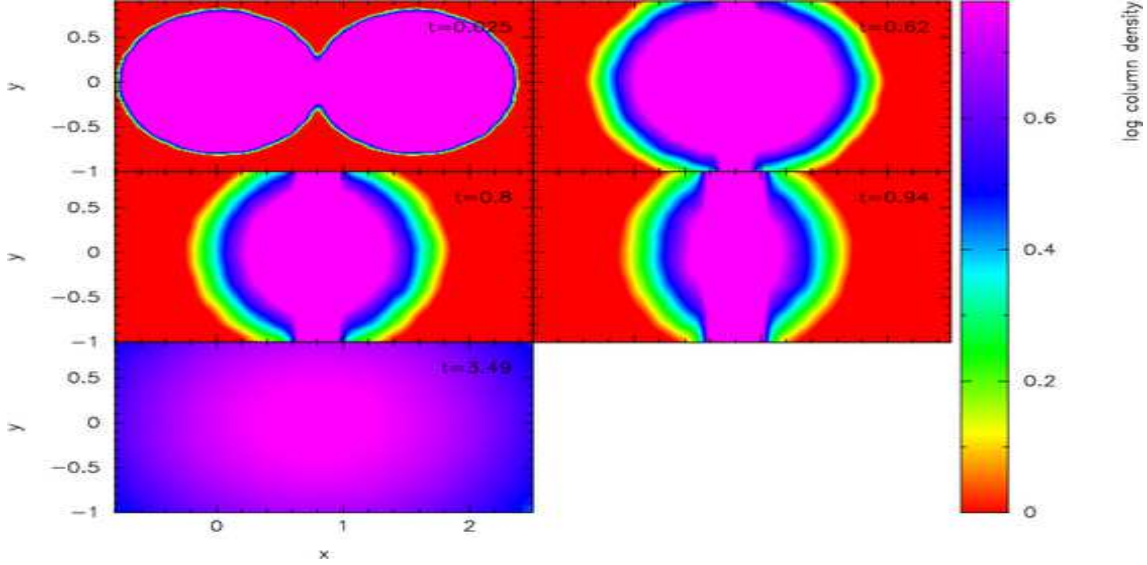


**Figure 1.** A column density plot of the time sequence of cloud collision in model 1. Post-collision, a pressure confined gas slab is formed which then re-expands and terminates in a diffuse gas cloud, as can be seen in the last snapshot,  $t = 3.49$  Myrs.

outcome of the simulation, since the temperature Jump condition will only provide a higher post-shock temperature, making the slab even warmer.

The post-shock gas slab in this model does not undergo gravitational fragmentation. After formation, it simply re-expands and ends up as a diffuse gas cloud ( $t = 3.49$  Myrs in Fig. 1). Unlike the gas slabs reported in paper I, the one in this model does not show any evidence for the bending instability. The evolution in this case appears more like an interplay between gravity and thermal pressure. There are two phases in this evolution. In the first, thermal pressure builds up in the slab after shocking and then, as the slab re-expands in the second, thermal pressure within it rapidly diminishes. The gravitational pressure also shows a similar pattern of evolution. Both, gravity and thermal pressure seem to be out of sync with each other during the formation and re-expansion; only in the terminal phases do they seem to be in phase. In Fig. 9 below, we plot evolution of the pressure (gravitational and thermal) against time, respective pressures have been normalised to unity.

The gas slab in this case is not sufficiently massive so as to become Jeans unstable. According to Whitworth *et al* (1994), the length of the fastest growing unstable mode is

$$L_{fastest} \sim \frac{2a_{layer}^2}{G\Sigma_{layer}}, \quad (6)$$

which is of order a few parsecs in the present case, atleast an order of magnitude larger than the slab thickness.

In model 2, we maintain physical conditions identical to those in the previous case except, that the cloud collision is now, off-centre. The impact parameter,  $b$ , is a fourth of the cloud radius,  $R_{cld}$ . The time sequence of colliding clouds

in this model is shown in Fig. 2. The cloud collision results in an oblique shocked slab unlike a planar slab in model 1. After formation, the slab tumbles about the  $z$ -axis and eventually re-expands, as in model 1. This can be seen in the snapshot corresponding to  $t = 1.89$  Myrs in Fig. 2.

As in model 1, the gas slab in this case also evolves through an interplay between the gravitational and thermal pressure. The curves tracing the respective pressures against time are very similar to those for model 1, as can be seen in Fig. 9. Contrary to intuition, the slabs in either cases evolve on a similar time timescale. The turnover in respective curves for gravitational and thermal pressure, in both models coincide. This suggests that the re-expansion of the oblique slab also commences at a similar epoch as the planar slab. Infact, the oblique slab expands slightly faster than the planar slab of model 1. This is evident from the plots in Fig. 9, where we can see that pressure in model 2 decreases faster than that in the latter model. This is presumably due to axial transfer of angular momentum as the outer ends of the oblique slab move outward (see snapshot corresponding to  $t = 1.89$  Myrs in Fig. 2).

Equation (6) above, is valid for off-centre cloud collision in the limit of a small impact parameter.  $L_{fastest}$ , calculated using this equation in the present case is much larger than the slab thickness. Hence as in model 1, the gas slab in this case as well, does not become Jeans unstable. Such a scenario (as in models 1 and 2) will thus, simply lead to formation of diffuse clouds in the galactic disk. These clouds may spawn star formation only when they have been sufficiently squeezed. Nonetheless, constituents of the galactic disk are replenished and recycled in the entire episode.

**Fast cloud collision ( $T_{ps} = 10$  K; models 3 & 4)**

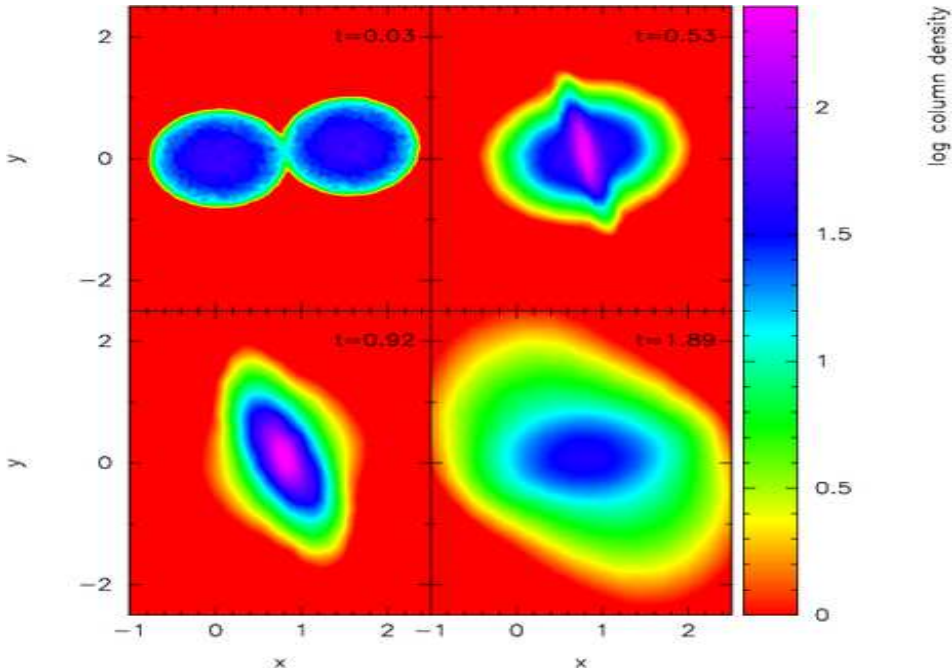


**Figure 2.** Column density plot showing a time sequence tracking model 2. This sequence shows the colliding clouds, formation of the post-collision gas slab and then its re-expansion.

We now repeat the simulations performed in models 1 and 2 in our next two models, 3 and 4 respectively, but with one change. We set the post-shock temperature,  $T_{ps}$ , equal to 10 K. As discussed above, we intend to explore the effect of cooling on the dynamical evolution of the gas slab. We saw in models 1 and 2 above, that the gas slab at 54 K was not susceptible to the gravitational instability.

However, in model 3, where the MCs collide head-on, we observe that the post-collision gas slab undergoes gravitational fragmentation. In Fig. 3, we present a time sequence of the gas slab after its formation, as seen face-on. As the gravitational instability starts growing, the slab shows signs of flocculation ( $t = 0.65$  Myr,  $t = 0.7$  Myr in Fig. 3), and eventually clumps in the slab condense out. Some of the smaller clumps merge to form larger clumps while some others lie embedded in filamentary structures. Most of the clumps being spheroidal, appear non-circular in the projection maps (see Fig. 4 below).

The gravitational instability grows on a time scale much smaller than the free fall time of the individual precollision clouds, or even the cloud crushing time,  $t_{cr}$ <sup>1</sup>. We now compare observations from this model with corresponding analytic predictions. In our simulation we observe that the

<sup>1</sup>  $t_{cr} = \frac{2R_{cld}}{v}$ , where  $v$  is the precollision speed of a cloud and  $R_{cld}$  is its radius.

clump formation commences after about 0.65 Myr. This is the time required for the growth of unstable mode,  $t_{growth}$ , leading to condensation of a clump and defined as,

$$t_{growth} \sim \left( \frac{L}{G\sigma_{layer} - a^2L^{-1}} \right)^{\frac{1}{2}} \quad (7)$$

(Whitworth *et al* 1994).

Here  $L$ ,  $\sigma_{layer}$ , and,  $a_{layer}$ , respectively are the size of the clump, average surface density of the slab, and the average sound speed in the slab. Plugging in the appropriate values from the simulation we get  $t_{growth} = 0.6$  Myr, which is in agreement with the epoch observed in the simulation. We again note that, clump formation commences after about 0.65 Myr. Thereafter the gravitational instability grows quickly and the slab fragments into a number of clumps. The minimum mass of a fragment is given by

$$M_{frag} = \mathcal{M}^{\frac{1}{2}} \frac{a_{layer}^3}{(G^3 \bar{\rho}_{layer})^{\frac{1}{2}}}, \quad (8)$$

Whitworth *et al* (1994). Here  $\bar{\rho}_{layer}$  is the average density of the layer and  $\mathcal{M}$  is the precollision Mach number. Using equation (8), we calculate the mass of this fragment,  $M_{frag}$ , as  $0.32 M_{\odot}$  ( $0.22 M_{\odot}$ ) for the present simulation. The number in brackets is the minimum mass of the fragment that condenses out of the slab.

The fragmentation of this slab results in the formation

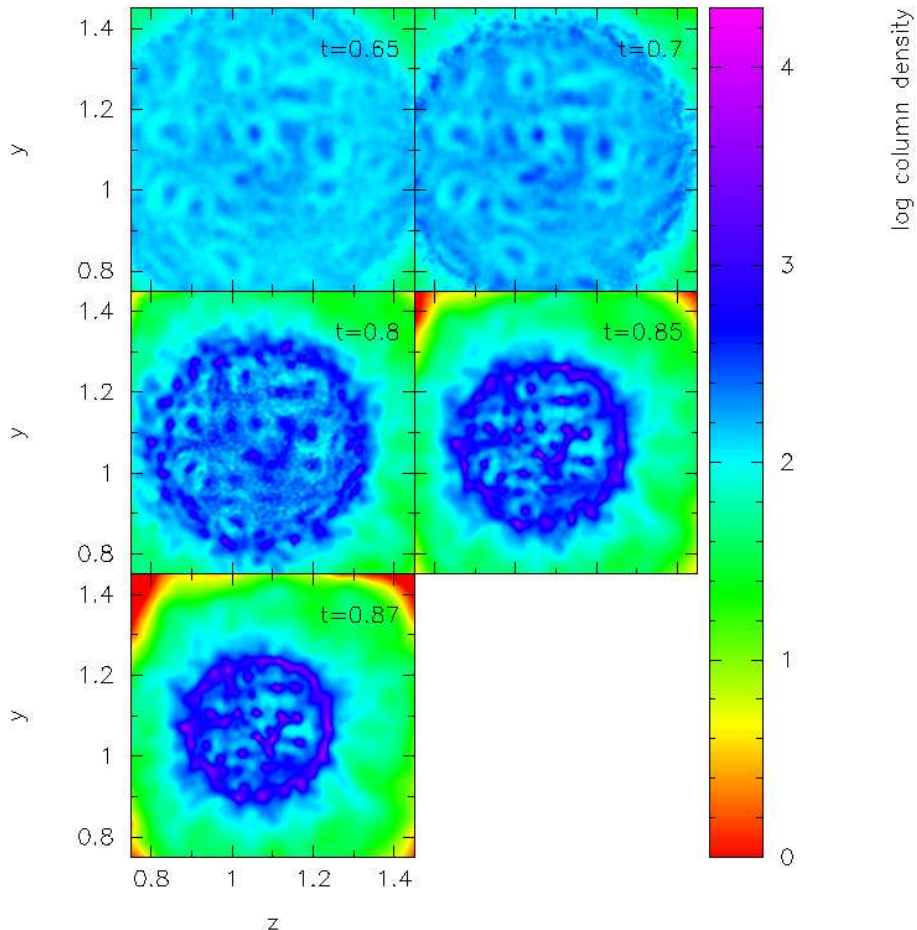


**Figure 3.** A sequence of contour plots showing the commencement of gravitational fragmentation, then clumping and finally fragmentation of the planar gas slab in model 3.

of 36 big and small clumps. Fig. 4 shows a close-up of the fragmented slab. At this epoch a few clumps have already become self gravitating while a few others, oscillate for some time before collapsing under self gravity. Fig. 5 shows a column density plot of the central region of this slab. Three sinks have been marked by black dots in as many clumps. Yet some other small clumps merge with similar clumps and form larger clumps and filaments. The column density plot in Fig. 4 shows a plethora of such structure in the fragmented slab. To facilitate identification of structure in the slab, we have overlaid density contours on the column density plot in this figure.

The slab as seen in Fig. 4 is fairly evolved and at this epoch, the gravitational instability has fully grown. Almost all of the gas in the slab ends up in density structures. The average density of the structure in the slab is  $\sim 10^{-18}$  g cm $^{-3}$ , which then suggests that the growth period of the instability as defined by Elmegreen (1989), and quoted above, is  $\sim 0.8$  Myr. This is comparable to the epoch (0.85 Myr) by which the instability has fully grown.

According to Nakamura, Hanawa & Nakano (1993), the characteristic length scale of a filamentary structure is

$$H = 0.0035 \left( \frac{a_{\text{layer}}}{0.3 \text{ km s}^{-1}} \right) \left( \frac{\bar{n}_{\text{layer}}}{2 \times 10^6 \text{ cm}^{-3}} \right)^{-\frac{1}{2}} \text{ pc}, \quad (9)$$

where all the symbols have their usual meanings. The average temperature of the densest regions in the slab is about

10K while  $\bar{n}_{\text{layer}} \sim 10^7$  cm $^{-3}$ . Plugging these values in equation (9) above, we get  $H \sim 0.13$  pc. The gravitational fragmentation of the filaments produce clumps and the separation between individual clumps is of the order of Jeans length,  $\lambda_J$ , which for a filament is  $\lambda_J \sim 22H$  (Nakamura, Hanawa & Nakano 1993). In the present case,  $\lambda_J \sim 0.3$  pc. This agrees with the average separation between clumps embedded in filamentary structures, as seen in Fig. (3) above. This simulation was terminated after  $t \sim 0.87$  Myr by which time seven sinks had formed in various clumps. Formation of self gravitating clumps is evident from the plot of pressure in Fig. 9 below.

Next, in model 4 the cloud collision produces an oblique gas slab confined by ram pressure. Like in the previous case (model 3), this slab also undergoes gravitational fragmentation. However, the fragmentation observed here is somewhat different from that reported by Chapman *et al* (1992) and Pongracic *et al* (1992). According to these authors, the oblique gas slab tumbles about a direction perpendicular to the plane of collision and breaks in to two blobs, which then undergoes secondary fragmentation to form multiples. Such a fragmentation resembles the bar mode instability. In the present case, although the oblique slab exhibits a similar tumbling motion the final outcome is different from that reported by the respective authors.

A possible reason for this observed difference could be, a smaller Jeans length in the present case. Our pre-collision

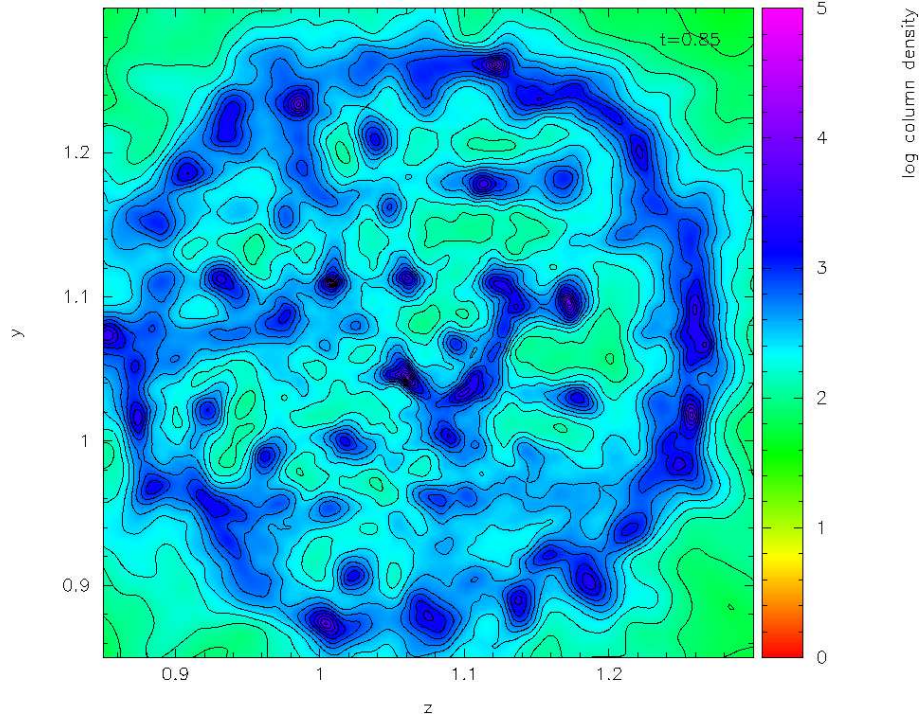


**Figure 4.** A column density plot of the fragmented slab in model 3. Density contours have been overlaid on it to facilitate identification of structure in it. A number of clumps and filaments can be seen in it.

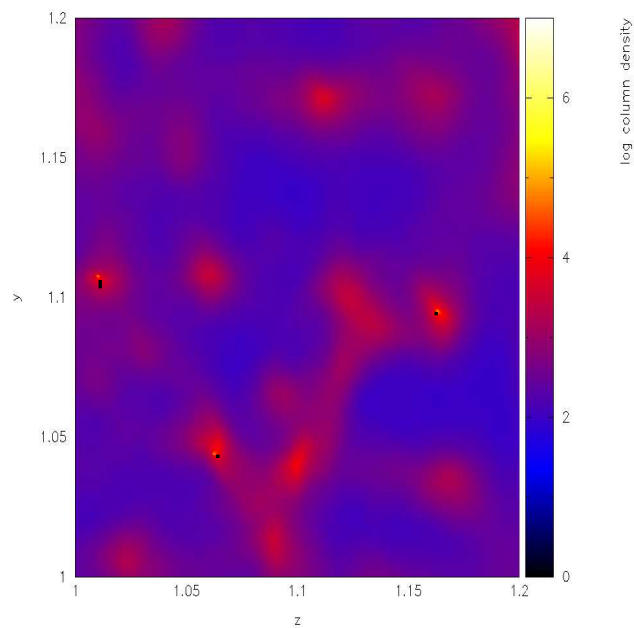


**Figure 5.** A column density plot showing a closer view of the central region of the fragmented slab in model 3. The (three) black dots are the (three) sinks formed in various clumps.

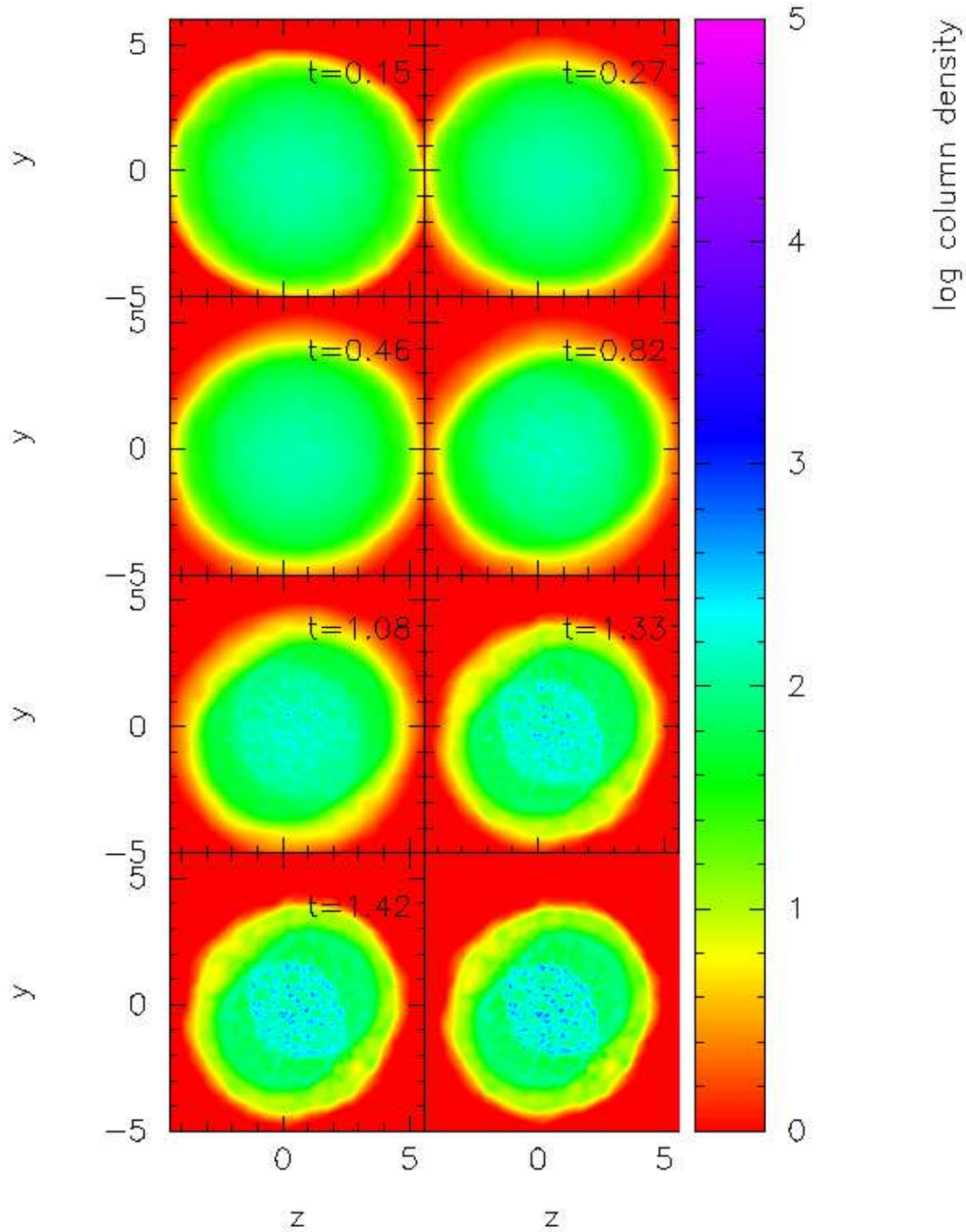


**Figure 6.** A time sequence of column density plots of the oblique slab in model 4. A face-on view of the slab has been shown in these plots. We can see that as the slab grows old, it shows signs of flocculation ( $t = 0.82$  Myr) and subsequently fragments (right hand plot in the third row,  $t = 1.6$  Myrs). The last plot shows a network of filaments and clumps embedded in them.

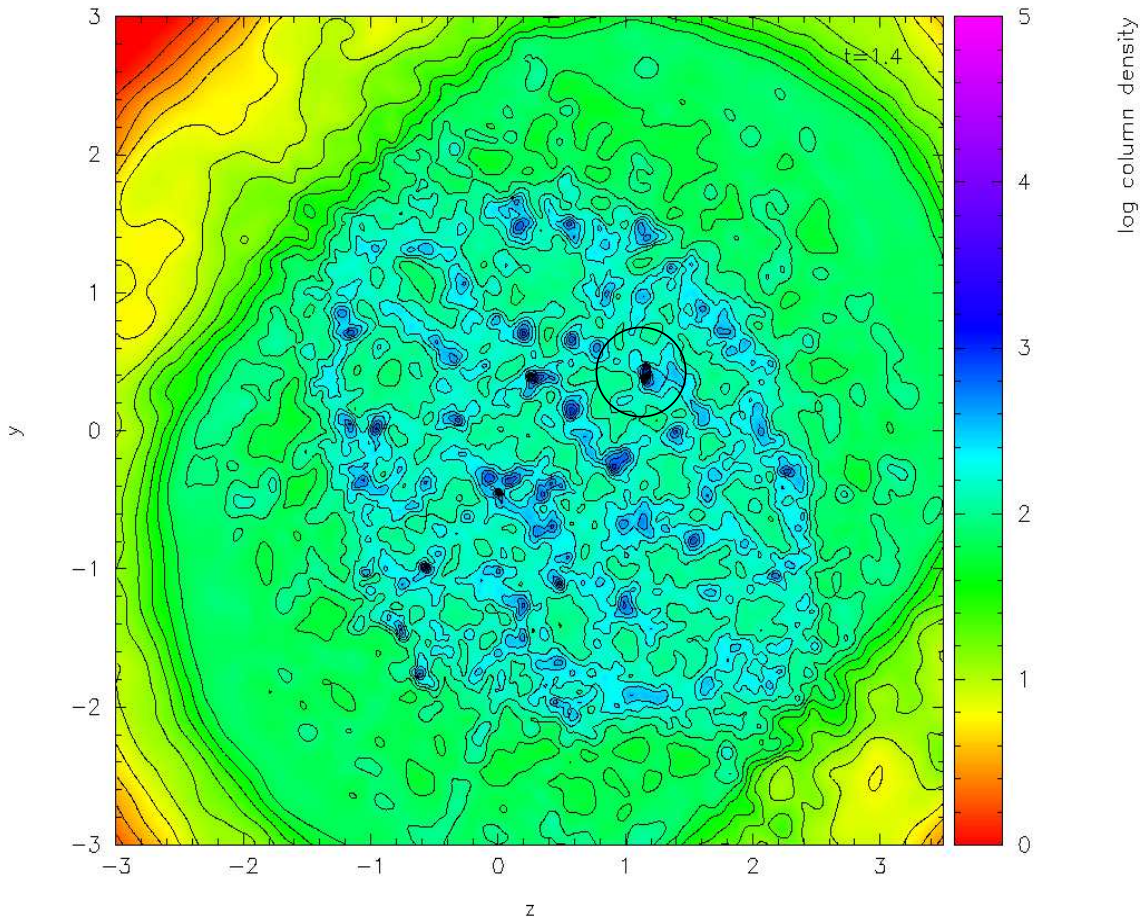


**Figure 7.** A contour plot showing more closely, the fragmented gas slab in model 4. Structure within the slab is evident with aid of the contours overlaid on this plot. Some clumps within the slab have become self gravitating. A clump that has undergone secondary fragmentation has been encircled.

clouds being more massive produce a slab with greater column density, which shortens the Jeans length and enhances its growth rate. In this eventuality, the gravitational instability will dominate over other unstable modes of the tumbling slab, notably the bar mode. The fragmentation of the slab after its formation can be seen in Fig. 6. This is a time sequence of column density plots of the gas slab, as seen face-on. The nature of fragmentation observed here is in consonance with the predictions of Whitworth *et al* (1994) for an off-centre cloud collision, with a small impact parameter.

As in the previous case, we calculated the dynamical properties for this slab, using equations (6), (7) and (8). Additionally, we also calculated the length of the fastest growing unstable mode in the slab,  $L_{fast}$ , defined as

$$L_{fast} = \frac{2a_{layer}^2}{G\sigma_{layer}} \quad (10)$$

Whitworth *et al*(1994). This is to check that the length of the fastest growing mode is, indeed much smaller than the radial extent of the slab. Clumping in the slab commences after  $\sim 0.4$  Myr, while the smallest clump has mass  $\sim 12 M_{\odot}$  and size  $\sim 0.1$  pc. Corresponding analytic calculations yield 0.4 Myr, 11  $M_{\odot}$  and 0.12 pc, respectively. The calculated values thus, seem to be in good agreement with those observed in the simulation.

Once the slab becomes unstable, it develops floccules and soon fragments. The final state of the slab, post-

fragmentation, can be seen in Fig. 7 which is a column density plot of the slab as seen face-on. The clumps and filaments in it have density of order  $10^{-19}$  g cm $^{-3}$ . Density contours have been overlaid on this plot to elucidate the structure in it.

We suggest fragmentation of cold gas slabs, as one of the mechanisms for clump formation and self gravitating clumps may spawn star clusters. A similar view was also presented by Clarke (1999). We have also seen that fragmentation of a gas slab produces elongated structure with clumps embedded in it. There is observational evidence for similar occurrences as has been reported, for instance by Lada, Alves & Lada (1999) and Elmegreen (2002) about a star cluster embedded in an elongated region, IC546. This cluster is thought to have been formed due to some dynamical trigger

#### Slow cloud collision

Finally, we examine the case of a very low velocity head-on cloud collision. As discussed above, an adiabatic EOS, given by equation (5) with  $\gamma = \frac{5}{3}$  is used to model the weak shock in this case. Fig. 8 shows a time sequence of column density plots of the colliding clouds. Post-collision, the clouds merge and form a prolate gas cloud ( $t = 1.42$  Myrs in Fig. 8). The cloud is thermally supported against self gravity. The thermal pressure gradient within the cloud is non-isotropic due to its aspherical shape.

Post-collision, as material from the colliding clouds

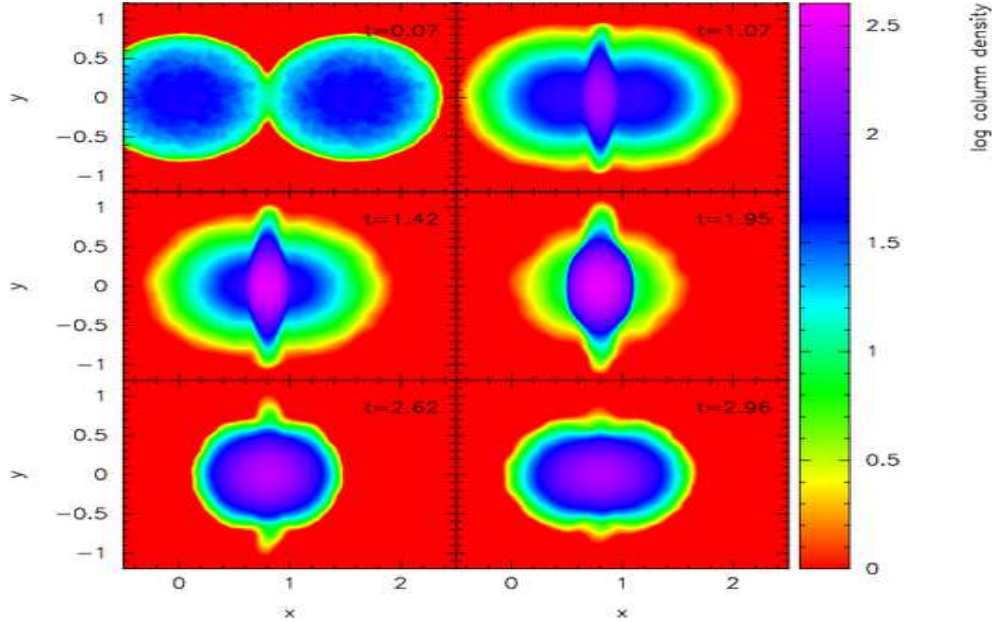


**Figure 8.** A sequence of column density plots in model 5. Collision of clouds, followed by the formation of a prolate gas cloud ( $t = 1.07$  Myrs) and then its re-expansion is evident from these plots. The expansion of the post-collision gas cloud terminates in a diffuse cloud ( $t = 2.96$  Myrs). Material squirting from the top and bottom ends (*jets*) of the slab are also visible in these plots.

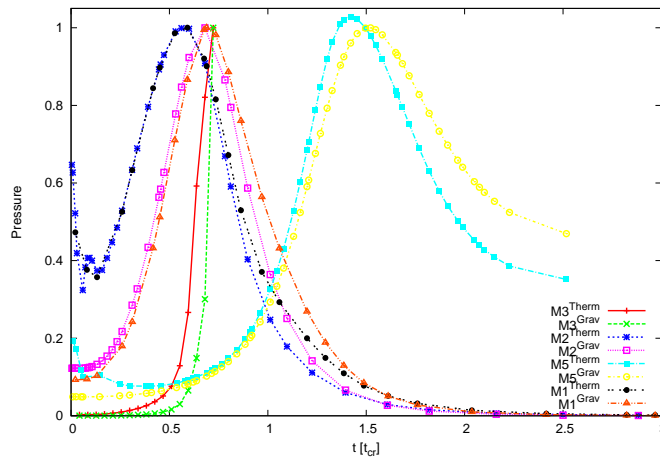


**Figure 9.** A plot showing the variation of pressure (gravitational and thermal) in models 1, 2, 3 and 5. The key in the right hand corner of the plot gives the model number and the corresponding identifiers for the respective curves.

streams in to the gas cloud, it progressively becomes denser and therefore warmer. This builds up a thermal reservoir within it, and the cloud, therefore starts re-expanding along the collision axis ( $t = 1.96$  Myrs,  $t = 2.62$  Myr and  $t = 2.96$  Myrs in Fig. 8). During this process it flattens, and

the re-expansion continues till the thermal pressure along the  $y$ -axis, arrests the lateral collapse. This observation in this simulation is in consonance with the qualitative predictions of Ramsay (1961) and Mestel (1965). Note that, the

cloud is not self gravitating and the lateral collapse is just a phenomenon involving gravo-thermal balance.

From the snapshots in Fig. 8, we can also see that some material is ejected, also called *jets*, from the top and bottom ends of the cloud. The qualitative feature of this model is similar to that of models 1 and 2 discussed above. However, the initial build up and the post-collision dissipation of thermal energy, happens much more slowly than in the previous cases, as is evident from the pressure plots in Fig. 9. We envisage such cloud collisions to lead to formation of diffuse clouds in the galactic disk. Star formation in such clouds can commence only when they become self gravitating or are suitably perturbed by density waves.

## 5 CONCLUSIONS

Colliding clouds dissipate kinetic energy and therefore must play an important role in the energy budget of the galactic disk. Cloud collision is a violent phenomenon and replenishes the elemental reservoir of the galactic disk. It is a prominent mechanism of triggered star formation and supposedly, also plays a pivotal role in the distribution of cloud masses and stellar population in the galactic disk (McKee 1999; Tan 2000).

In the present work, having explored the paradigm of low velocity cloud collisions, we have also tried to ascertain the importance post-shock cooling alibi, in a rather crude manner, on the dynamical evolution of the pressure confined slab. Our simple investigation of this matter suggests that, under suitable conditions, gas slabs become Jeans unstable and fragment to produce clumps and filaments. We conclude that colder slabs are more likely to fragment otherwise, the slab simply re-expands and ends up as a diffuse cloud.

The former scenario is more interesting from the perspective of star formation, either multiples or larger  $N$ -body clusters. Density perturbations in the gas slab grow purely from white noise and therefore do not require any external trigger. In the latter scenario however, the diffuse gas clouds may become self gravitating, when crushed by sufficient external pressure else, clouds of various shapes simply lie scattered in the interstellar medium of the galactic disk.

Models 1, 2, and 5 in the present work, belong to this latter paradigm while models 3 and 4, to the former. Figs. 4 and 7 respectively, show the fragmented gas slabs in models 3 and 4. Clumps and well defined, elongated density structures are evident in both. Indeed, a few clumps in both, have become self gravitating by the time respective calculations were terminated. The collapse of individual clumps however, could not be followed further due to shortage of resources. However, fragmentation of gas slabs is evidently a propitious mode of clump formation. Clumps may eventually spawn stars and larger clouds may become wombs for larger star clusters.

The results of our off-centre cloud collision experiments (both models 2 and 4) differ significantly from similar experiments performed by Lattanzio *et al* (1985), Chapman *et al* (1992) and Bhattal *et al* (1998) among others. These authors report a bar mode fragmentation of the post-collision oblique pressure compressed slab, which is different from the fragmentation observed in our model. On the contrary, we observe that the oblique gas slab either, simply re-expands

to finally produce a diffuse gas cloud (model 2) or, fragments gravitationally to form clumps and filaments (model 4). We attribute this difference to the fact that the mass of the slab which, in our simulation is atleast an order of magnitude greater than that in the work cited above. As a result of larger mass and therefore higher column density, the length of the unstable mode is shortened and grows much faster.

We admit that the investigation presented here is too simplified and dwells purely on a gravo-thermal treatment of the problem. At best, we have a skewed picture before us for a more more elaborate future study. For a more complete treatment of the subject, magnetic field needs to be included and post-shock radiative cooling needs to be better treated (*c. f.* Vázquez-Semadeni *et al* 2007). Also, collapsing clumps can be followed further by employing a radiative transfer scheme (*c. f.* Stamatellos *et al* 2007), rather than a simple barotropic EOS used here.

## 6 ACKNOWLEDGMENTS

This work was completed as part of post graduate research and funded through a studentship (DSW/Edu/Inf/2004/6283(35)) awarded by the State Government Of Maharashtra, India. All the column density plots presented here were prepared using the publicly available graphics package, SPLASH prepared by Dr. D. Price (Price 2007). Dr. S. V. Anathpindika specially thanks Dr. Simon Goodwin for providing the latest version of his SPH code, DRAGON.

## REFERENCES

- Anathpindika, S. (*MNRAS submitted*) arXiv 0810.5011v3
- Barnes, J & Hut, P., 1986, *Nature*, 324, 446
- Bate, M., Bonnell, I., Price, N., 1995, *MNRAS*, 277, 362
- Boyd, D & Whitworth, A., 2005, *A&A*, 430, 1059
- Bhattal *et al*, 1998, *MNRAS*, 297, 435
- Block *et al*, 1994, *A&A*, 288, 365
- Chapman *et al*, 1992, *Nature*, 359, 207
- Clarke, C., 1999, *MNRAS*, 307, 328
- Clarke, C & Gittins, D., 2006, *MNRAS*, 371, 530
- Clarke, C., Bonnell, I & Hillenbrand, L., 2000, *Protostars And Planets iv*, Eds. Mannings, V., Boss, A & Russell, S., Arizona Press
- Curry, C., 2002, *ApJ*, 576, 849
- Dale, J., Bonnell, I & Whitworth, A., 2007, *MNRAS*, 375, 1291
- Elmegreen, B & Elmegreen, D, 1978, *ApJ*, 220, 1051
- Elmegreen, D & Elmegreen, B, 1986, *ApJ*, 311, 554
- Elmegreen, B, 1989, *ApJ*, 340, 786
- Elmegreen, B., *IAU Symposium Series, Extragalactic Star Clusters*, Vol. 207, Eds. Geisler, D., Grebel, E & Minniti, D., 2002
- Furuya, R., Kitamura, Y., & Shinnaga, H., 2008, *PASJ*, 60, 421
- Goodwin, S. & Whitworth, A., Ward-Thompson, D., 2004, *MNRAS*, 414, 633
- Hoyle, F., 1953, *ApJ*, 118, 513
- Kennicutt, R., 1989, *ApJ*, 344, 685
- Kennicutt, R., 1998, *ApJ*, 498, 541

- Klessen, R., Burkert, A. & Bate, M., 1998, *ApJLett*, 501, L205
- Klessen, R. & Burkert, A., 2000, *ApJSS*, 128, 287
- Lada, C., Alves, J. & Lada, B., 1999, *ApJ*, 512, 250
- Larson, R., 1985, *MNRAS*, 214, 379
- Lattanzio *et al*, 1985, *MNRAS*, 215, 125
- Lefloch, B., Cernicharo, J., & Pardo, J., 2008, *A&A* submitted, arXiv 0809.2023v1
- Makino, J., 1991, *PASJ*, 43, 859
- McKee, C., 1999, *Conf. Proc. The Physics Of Star Formation & Early Stellar Evolution*, arXiv 9901370
- Mestel, L., 1965, *QJRAS*, 6, 161
- Meyer, M. & Lada, E., 1999, *The Stellar Populations In L1630 (Orion B) Cloud*. In *'The Orion Complex Revisited'*, ASP Conf. Ser. Ed. McCaughrean, M
- Mookerjee *et al*, 2000, *AJ*, 120, 1954
- Nakamura, F., Hanawa, T. & Nakano, T., 1993, *PASJ*, 45, 551
- Pongracic *et al*, 1992, *MNRAS*, 256, 291
- Price, D., 2007, *PASA*, 24(3), 159
- Pudritz, R., 2002, *Science*, 295, 68
- Ramsay, A., 1961, *Theory Of Newtonian Attraction*; Cambridge University Pub.
- Schmidt, M., 1959, *ApJ*, 129, 243
- Stamatellos *et al*, 2007, *AA*, 475, 37
- Tan, J., 2000, *ApJ*, 536, 173
- Vázquez-Semadeni *et al*, 2007, *ApJ*, 657, 780
- Wada, K., Spaans, M., & Kim, S., 2000, *ApJ*, 540, 797
- Whitworth *et al* 1994, *A&A*, 290, 421
- Whitworth *et al* 1996, *MNRAS*, 283, 1061
- Wyse, R., 1986, *ApJ*, 311, L41
- Wyse, R. & Silk, J., 1989, *ApJ*, 339, 700